Supplementary Information for Elastohydrodynamic scaling law for heart rates by

E. Virot, V. Spandan, L. Niu, W. van Rees, and L. Mahadevan

SCALING LAW FOR HEART RATE WHEN DOMINATED BY STRETCHING

To complement the discussion in the main text, here we consider the case of a (thin) shell dominated by stretching deformations. The work required to deform such a shell scales as $E\epsilon^2 R^2 h$, where E is the elastic modulus of the walls and $\epsilon \sim A/R$ is the stretching strain for a small amplitude of deformation A. This work is converted into kinetic energy of the fluid that is pushed out, and scales as $\rho_\mathrm{f} R^3 (A f_\mathrm{t})^2$, where we have assumed that the fluid velocity scales as the product of the frequency f_t and the amplitude A. Balancing the work and kinetic energy yields an estimate for the frequency of such a fluid-loaded & purely stretched soft elastic shell as

$$f_\mathrm{t} \approx \frac{c'_\mathrm{shape}}{2\pi} \sqrt{\frac{E}{\rho_\mathrm{f}}}\, \frac{h^{1/2}}{R^{3/2}}, \tag{S1}$$

where c'_shape is a dimensionless constant that is determined by the shape of the ventricle ($c'_\mathrm{shape} \simeq \sqrt{3}$ for a sphere, and $c'_\mathrm{shape} \simeq \sqrt{2}$ for a cylinder). We note that the scaling law is qualitatively different from the estimate obtained by balancing the bending energy and the kinetic energy (see (1) in the main text) - differing by a factor of h/R. For the dimensions of a human heart, $h \sim 10\,\mathrm{mm}$, $R \sim 30\,\mathrm{mm}$, $E \sim 10^4\,\mathrm{Pa}$ and $\rho_\mathrm{f} \sim 10^3\,\mathrm{kg/m^3}$, which gives an elastohydrodynamic resonance frequency $f_\mathrm{t} \sim 10\,\mathrm{Hz}$, larger than the one obtained when deformations dominated by bending by a factor $\sqrt{12}R/h$. For twist-driven pumping that is the typical mode of ventricular deformation, the shell deforms primarily via twist-induced buckling that leads to bending, so that the scaling law (1) in the main text is the appropriate one to characterize resonant pumping in the heart.

NUMERICAL SIMULATIONS

Elasticity

In order to simulate the twist induced buckling of the cylindrical shell, we minimize the elastic energy for Kirchhoff-Love shells [1]. This energy can be written in terms of the first fundamental form a and second fundamental form b of the mid-surface in the current configuration and the reference configuration (denoted by the subscript 0):

$$\mathcal{E} = \frac{1}{2}\int_U \left[\frac{h}{4}\left\|a_0^{-1}a - I\right\|_e^2 + \frac{h^3}{12}\left\|a_0^{-1}\left(b - b_0\right)\right\|_e^2\right]\sqrt{\det a_0}\; dx\; dy, \tag{S2}$$

The integral is evaluated over the range of parametric coordinates $(x, y) \in U \subset \mathbb{R}^2$, where U defines the parametric domain whose mapping to $\mathbb{R}^3$ corresponds to the mid-surface embedding. The elastic norm $\|\mathbf{A}\|_e^2 = \alpha \mathrm{Tr}^2(\mathbf{A}) + 2\beta \mathrm{Tr}(\mathbf{A}^2)$ defines the invariants of the strain $\mathbf{A}$, with the coefficients $\alpha = E\nu_p/(1-\nu^2)$ and $\beta = E/(2+2\nu_p)$ being the plane-stress Lamé parameters expressed in terms of the Young's modulus E and Poisson's ratio ν_p, of the St. Venant-Kirchhoff material model. We note that, for a thin plate ($b_0 = 0$), when the assumptions of moderate rotations and small in-plane strain assumptions are explicitly taken into account. this energy reduces to the Föppl-van Karman energy [2].

For our discrete approximation of the shell, the first and second fundamental forms of the mid-surface can be written as

$$a_\mathrm{triangle} = \begin{pmatrix} \vec{e}_1 \cdot \vec{e}_1 & \vec{e}_1 \cdot \vec{e}_2 \\ \vec{e}_1 \cdot \vec{e}_2 & \vec{e}_2 \cdot \vec{e}_2 \end{pmatrix}$$

$$b_\mathrm{triangle} = \begin{pmatrix} 2\vec{e}_1 \cdot (\vec{n}_0 - \vec{n}_2) & -2\vec{e}_1 \cdot \vec{n}_0 \\ -2\vec{e}_1 \cdot \vec{n}_0 & 2\vec{e}_2 \cdot (\vec{n}_1 - \vec{n}_0) \end{pmatrix}$$

where $\vec{e}_i$ represent directed edges of the triangle, and $\vec{n}_i$ represent normal vectors defined on all edges of the triangle mesh. The introduction to edge-normal vectors introduces extra degrees of freedom into the mesh; see [1] for an

exposition of this choice. This leads to a discretized expression of the elastic energy as a sum over all triangular faces, as further detailed in [1, 2]. The total energy is then minimized with respect to all free mesh vertex positions and the orientation of edge-normal vectors, given the rest configuration and appropriate loading/boundary conditions. The current implementation uses the L-BFGS method to minimize the total energy.

Hydrodynamics

The cylindrical shell is immersed in a fluid, the dynamics of which are computed by solving the incompressible Navier-Stokes equations in a three-dimensional Cartesian domain:

$$\frac{\partial \mathbf{u}}{\partial t} + \mathbf{u} \cdot \nabla \mathbf{u} = -\frac{1}{\rho_{\mathrm{f}}} \nabla p + \nu \nabla^2 \mathbf{u} + \mathbf{f}^{\mathrm{ibm}}, \tag{S3}$$

$$\nabla \cdot \mathbf{u} = 0. \tag{S4}$$

where $\mathbf{u}$ is the fluid velocity vector, ρ_{f} is the density of the fluid and p is the hydrodynamic pressure. $\mathbf{f}^{\mathrm{ibm}}$ is the force needed to enforce the influence of the cylindrical shell on the flow through the immersed boundary method. In the immersed boundary method the boundary condition of any immersed surface (here no-slip) is represented through a momentum source in the governing momentum equations. The equations are solved using an energy-conserving second-order centered finite difference scheme in a Cartesian domain with fractional time-stepping. An explicit Adams-Bashforth scheme is used to discretise the non-linear terms while an implicit Crank-Nicholson scheme is used for the viscous terms. Time integration is performed via a self starting fractional step third-order Runge-Kutta (RK3) scheme. Additional details on the numerical schemes and validation can be found in [9, 10]. The simulations are run in such a way that hydrodynamic stresses do not influence the structural dynamics. This allows us to explicitly test the dependence of pumping dynamics on the twist-untwist frequency.

Dynamics of pumping

In the attached Supplementary movie S1, we show animations of the pumping dynamics when the shell is immersed in the fluid. The dotted lines represent the domain and the flow is visualised in the mid-plane bisecting the cylindrical shell. The colour represents the velocity of the fluid in the axial direction.

EXPERIMENTS ON TWIST BUCKLING OF A CYLINDRICAL SHELL

To realise this experimentally, we build a model of a tubular heart-like pump made of an elastomer that ejects fluid by twisting and bending. The cylindrical shell of constant thickness $h = 2.3$ mm and radius $R = 18.9$ mm is obtained by spincasting a curing solution of silicone at 1000 rpm in a cylindrical mold. The geometry of the shell is characterised by the aspect ratio L/R and thickness ratio R/h, where L, R and h are the length, radius and thickness of the shell, respectively. The shape evolution of such a shell is shown in Fig. S1. Such a device can yield ejection fractions of 50% with bending strains smaller than 30%, as shown in Fig. S2.

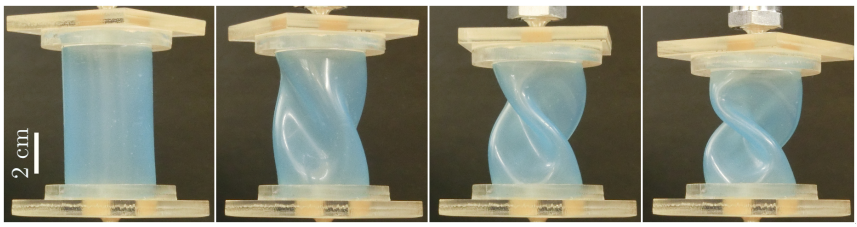

FIG. S1. Artificial pump undergoing controlled instabilities under twist. The shell thickness is $h = 2.3$ mm, its radius is $R = 18.9$ mm, $R/h \simeq 8.2$.

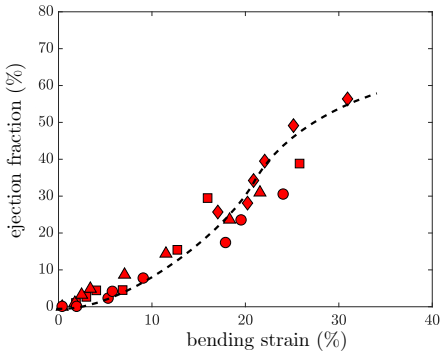

FIG. S2. Ejection fraction as a function of the maximum bending strain of the shell, measured experimentally by determining the radius of curvature of the wrinkles. The different symbols indicate four independent series of tests. The dashed line is a guide for eyes.

HEART SIZE, SHAPE AND RATE DATA

Here we report the references that have been used in Fig. 3 of the main text. R denotes the radius of the left ventricle at the end of the diastole regime. h denotes the average thickness of the left ventricle at the end of the diastole regime. The reported value of the heart rate, f_e, is an average on adult male and female specimens. In an individual, the heart rate f_e varies as a function of the temperature, stress level, physical activity, disease. Nevertheless, we made the choice to only report the average value for the healthy adult animal. In [11], the wall thickness h is estimated from measurements of the end-diastole volume of the left ventricle and from the myocardial volume.

TABLE S1. Heart geometry and heart rate in terrestrial mammals. (*) The Etruscan shrew heart wall thickness is estimated from the value of R and the best fit $h = 0.21 \times R^{1.15}$ indicated in Fig. S3.

		R (mm)	h (mm)	R/h	f_e (Hz)	sources
Etruscan shrew	*Suncus etruscus*	0.8	0.2*	4.9*	16.7	[12]
Mouse	*Mus musculus*	2.8	0.8	3.5	9.7	[5, 120, 199, 207] in [11]
Rat	*Rattus norvegicus*	3.8	1.9	2.1	5.1	[13]
Rat	*Rattus rattus*	5.1	2.1	2.4	5.7	[56, 87, 88, 106, 113, 127, 134, 136, 177] in [11]
Guinea pig	*Cavia porcellus*	7.2	1.8	4.0	4.6	[7, 81, 83, 87, 107, 132, 167] in [11]
Cat	*Felis domesticus*	11.7	4.8	2.4	3.0	[19, 35, 78, 103, 115, 138] in [11]
Three-toed slot	*Bradypus tridactylus*	11.9	3.1	3.8	1.4	[21, 38, 39, 40, 138] in [11]
Domestic rabbit	*Oryctolagus cuniculus*	12.1	2.5	4.8	4.2	[18, 34, 49, 104, 117, 154, 190] in [11]
Rhesus monkey	*Macaca mulatta*	12.6	4.1	3.1	2.6	[27, 54, 55, 191] in [11]
Cynomolgus monkey	*Macaca fascicularis*	14.3	6.2	2.3	2.9	[27, 30, 100] in [11]
Dog	*Canis familiaris*	27.3	8.7	3.1	1.8	[6, 17, 44, 81, 88, 98, 127, 135, 141, 171, 175, 203, 204] in [11]
Euro kangaroo	*Macropus robustus*	29.4	16.2	1.8	1.5	[121] in [11]
Goat	*Capra hircus*	32.9	8.9	3.7	1.3	[88] in [11]
Human	*Homo sapiens*	33.7	7.1	4.7	1.2	[4, 7, 11, 16, 44, 59, 91, 111, 127, 145, 202] in [11]
Sheep	*Ovis aries*	40.0	8.4	4.8	2.1	[24, 44, 51, 88, 125] in [11]
Pig	*Sus scrofa*	42.1	10.8	3.9	1.4	[88, 169, 200] in [11]
Llama	*Lama glama*	45.9	10.9	4.2	1.0	[4, 41, 60] in [11]
Camel	*Camelus dromedarus*	62.6	18.6	3.4	1.0	[92, 126] in [11]
Cattle	*Bos taurus*	69.1	19.1	3.6	1.0	[88, 95] in [11]
Horse	*Equus caballus*	75.9	28.6	2.7	0.8	[48, 58, 88, 95, 124] in [11]
Giraffe	*Giraffa camelopardalis*	91.0	55.9	1.6	1.7	[193] in [11]
Asian elephant	*Elephas maximus*	134.0	48.4	2.8	0.5	[9, 89] in [11]
African elephant	*Loxodonta africana*	149.5	52.6	2.8	0.7	[89] in [11]

[1] C. Weischedel, A. Tuganov, T. Hermansson, J. Linn, M. Wardetzky Construction of discrete shell models by geometric finite differences (Fraunhofer ITWM, Kaiserslautern, Germany), Technical Report **220** (2012).

[2] W. M. van Rees, E. Vouga, L. Mahadevan Growth patterns for shape-shifting elastic bilayers *Proceedings of the National Academy of Sciences, USA* **114**, 11597-11602 (2017).

[3] F. P. Mall, On the muscular architecture of the ventricles of the human heart, *The American Journal of Anatomy* **2**, 211-266 (1911).

[4] R. A. Greenbaum, S. Y. Ho, D. G. Gibson, A. E. Becker, R. H. Anderson, Left ventricular architecture in man, *British Hear Journal* **45**, 248-263 (1981).

[5] F. Torrent-Guasp, Estructura y funcion del corazon, *Revista Espanola de cardiologia* **51**, 91-102 (1998).

TABLE S2. Heart geometry and heart rate in marine mammals and birds. (*) The hummingbird heart wall thickness and the blue whale left ventricle radius are estimated from the value of R and the best fit $h = 0.21 \times R^{1.15}$ indicated in Fig. S3.

	R (mm)	h (mm)	R/h	f_e (Hz)	sources
Dolphin	*Tursiops truncatus*	37.7	21.1	1.8	2.0	[178] in [11]
Harbor seal	*Phoca virtulina*	38.9	15.9	2.4	1.6	[102] in [11]
Blue whale	*Balaenoptera musculus*	200.0*	94.0	4.4*	0.3	[14, 15]

	R (mm)	h (mm)	R/h	f_e (Hz)	sources
Hummingbird	*Archilochus colubris*	1.5	0.3*	4.4*	10.3	[16, 17]
Canary	*Serinus serinus*	2.8	1.3	2.1	9.0	[137, 207] in [11]
House sparrow	*Passer domesticus*	3.5	1.7	2.0	7.4	[10, 137] in [11]
Starling	*Sturnus vulgaris*	4.6	2.3	2.0	6.3	[207] in [11]
Robin	*Turdus migratorius*	4.8	2.1	2.3	8.7	[207] in [11]
Quail	*Coturnix coturnix*	5.5	2.1	2.6	8.5	[159] in [11]
Pigeon	*Columba livia*	8.2	2.9	2.8	3.1	[10, 71, 82, 161] in [11]
Chicken	*Gallus gallus*	9.4	4.5	2.1	5.1	[142, 186, 187, 197] in [11]
Duck	*Anas platyrhynchos*	13.2	4.8	2.7	2.8	[22, 71, 93, 94, 184] in [11]
Turkey	*Meleagris gallopavo*	15.4	2.6	5.9	2.7	[8, 170] in [11]
Emu	*Dromaius novaehollandiae*	34.3	14.0	2.5	0.8	[70] in [11]
Ostrich	*Struthio camelus*	50.9	24.0	2.1	0.9	[28, 29] in [11]

[6] F. Torrent-Guasp, G. D. Buckberg, C. Clemente, J. L. Cox, H. C. Coghlan, M. Gharib, The structure and function of the helical heart and its buttress wrapping, *Seminars in Thoracic and Cardiovascular Surgery* 13, 301-319 (2001).

[7] M. J. Kocica, A. F. Corno, V. Lackovic, V. I. Kanjuh, The helical ventricular myocardial band of Torrent-Guasp, *Pediatric Cardiac Surgery Annual* , 52-60 (2007).

[8] T. Arts, S. Meerbaum, R.S. Reneman, E. Corday, Torsion of the left ventricle during the ejection phase in the intact dog, *Cardiovascular Research* **18**, 183-193 (1984).

[9] V. Spandan, V. Meschini, R. Ostilla-Monico, D. Lohse, G. Querzoli, M. D. de Tullio, R. Verzicco A parallel interaction potential approach coupled with the immersed boundary method for fully resolved simulations of deformable interfaces and membranes, *Journal of Computational Physics* **348**, 567-590 (2017).

[10] V. Spandan, D. Lohse, M. D. de Tullio R. Verzicco A fast moving least squares approximation with adaptive Lagrangian mesh refinement for large scale immersed boundary simulations, *Journal of Computational Physics* **375**, 228-239 (2018).

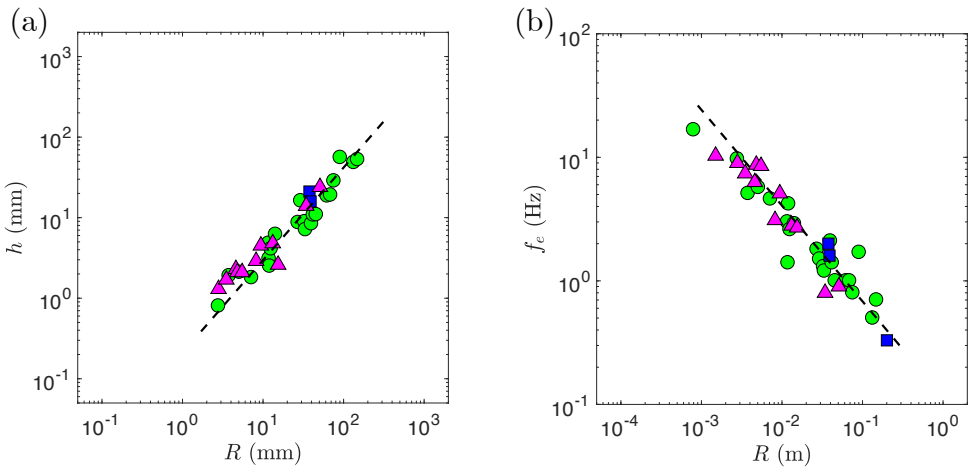

FIG. S3. Left and right panels shows typical wall thickness h of the left ventricle and the experimentally measured heart rate $f_{\rm e}$ as a function of the typical radius R of the left ventricle, respectively. The reported values are the averaged ones (see S.I.). The best fit is given by $h = C_h R^{1.15}$, where h and R are expressed in millimeters (dashed line), and the dimensional constant $C_h = 0.21 mm^{-.15}$. The corresponding prediction in terms of heart rate is given by $f_{\rm e} = f_{\rm t} = C_f R^{-0.78}$, where $f_{\rm e}$ and R are expressed in Hertz and meters respectively (dashed line), and the dimensional constant $C_f = 0.11 Hz.m^{1.78}$. The values of these parameters are averaged over the diastole and the systole. Green circles are terrestrial mammals, blue squares are marine mammals and magenta triangles are birds.

[11] R. S. Seymour, A. J. Blaylock, The principle of Laplace and scaling of ventricular wall stress and blood pressure in mammals and birds, *Physiological and Biomedical Zoology* **73**, 389-405 (2000).

[12] R. Fons, S. Sender, T. Peters, K. D. Jurgens, Rates of rewarming, heart and respiratory rates and their significance for oxygen transport during arousal from torpor in the smallest mammal, the Etruscan shrew *Suncus etruscus*, *Journal of Experimental Biology* **200**, 1451-1458 (1997).

[13] C. Weytjens, B. Cosyns, J. D'Hooge, C. Gallez, S. Droogmans, T. Lahoute, P. Franken, G. Van Camp, Doppler myocardial imaging in adult male rats: Reference values and reproducibility of velocity and deformation parameters, *European Journal of Echocardiography* **7**, 411-417 (2006).

[14] G. J. Race, W. L. J. Edwards, E. R. Halden, H. E. Wilson, F. J. Luibel, A large whale heart, *Circulation* **19**, 928-932 (1959).

[15] B. Singh, Morbidity and mortality in cardiovascular disorders: impact of reduced heart rate, *Journal of Cardiovascular Pharmacology and Therapeuticst* **6**, 13-33 (2001).

[16] E. P. Odum, The heart rate of small birds *Science* **101**, 153-154 (1945).

[17] R.A. Norris, C.E. Connell and D.W. Johnston Notes on fall plumages, weights, and fat condition in the ruby-throated hummingbird, *The Wilson Bulletin* **69**, 155-163 (1957).